

## Article

# Planar Perovskite Solar Cells Using Perovskite CsPbI<sub>3</sub> Quantum Dots as Efficient Hole Transporting Layers

Tsair-Chun Liang <sup>1</sup>, Hsin-Yu Su <sup>1</sup>, Sih-An Chen <sup>2,3</sup>, Yen-Ju Chen <sup>4</sup>, Chung-Yu Chiang <sup>2</sup>, Chih-Hsun Chiang <sup>2</sup>, Tzung-Ta Kao <sup>1</sup>, Lung-Chien Chen <sup>2,\*</sup> and Chun-Cheng Lin <sup>3,\*</sup>

<sup>1</sup> Institute of Photonics Engineering, National Kaohsiung University of Science and Technology, Kaohsiung 824005, Taiwan

<sup>2</sup> Department of Electro-Optical Engineering, National Taipei University of Technology, Taipei City 106344, Taiwan

<sup>3</sup> Department of Mathematic and Physical Sciences, R.O.C. Air Force Academy, Kaohsiung 820008, Taiwan

<sup>4</sup> Department of Electronic Engineering, Ming Chi University of Technology, New Taipei City 243303, Taiwan

\* Correspondence: ocean@ntut.edu.tw (L.-C.C.); cclincafa@gmail.com (C.-C.L.)

**Abstract:** Perovskite CsPbI<sub>3</sub> quantum dots (QDs) were synthesized as a hole-transporting layer (HTL) of a planar perovskite solar cell (PSC). By using the Octam solution during the ligand engineering, CsPbI<sub>3</sub> QDs exhibits a denser grain and a larger grain size due to the short-chain ligands of Octam. In addition, CsPbI<sub>3</sub> QDs with the Octam solution showed a smooth and uniform surface on MAPbI<sub>3</sub> film, indicating the QDs improved the microstructure of the MAPbI<sub>3</sub> perovskite film. As a result, the PSC with CsPbI<sub>3</sub> QDs as an HTL has the optimal open-circuit voltage as 1.09 V, the short-circuit current as 20.5 mA/cm<sup>2</sup>, and the fill factor (FF) as 75.7%, and the power conversion efficiency (PCE) as 17.0%. Hence, it is inferred that introducing QDs as a HTL via the ligand engineering can effectively improve the device performance of the PSC.



**Citation:** Liang, T.-C.; Su, H.-Y.; Chen, S.-A.; Chen, Y.-J.; Chiang, C.-Y.; Chiang, C.-H.; Kao, T.-T.; Chen, L.-C.; Lin, C.-C. Planar Perovskite Solar Cells Using Perovskite CsPbI<sub>3</sub> Quantum Dots as Efficient Hole Transporting Layers. *Materials* **2022**, *15*, 8902. <https://doi.org/10.3390/ma15248902>

Academic Editor: Antonio Agresti

Received: 26 October 2022

Accepted: 6 December 2022

Published: 13 December 2022

**Publisher's Note:** MDPI stays neutral with regard to jurisdictional claims in published maps and institutional affiliations.



**Copyright:** © 2022 by the authors. Licensee MDPI, Basel, Switzerland. This article is an open access article distributed under the terms and conditions of the Creative Commons Attribution (CC BY) license (<https://creativecommons.org/licenses/by/4.0/>).

**Keywords:** perovskite; quantum-dot (QD); nanoparticle (NP); perovskite solar cell (PSC)

## 1. Introduction

Economic growth and industrialization have led to increased use of fossil fuels. Increased production and consumption of fossil fuels has had several adverse environmental impacts on the countries, including global warming, air pollution and increased health risks [1]. Therefore, the promotion of renewable energy is imperative and the International Energy Agency (IEA) released a roadmap for realizing net-zero carbon dioxide (CO<sub>2</sub>) emissions in the energy sector by 2050 [2]. Among renewable energies, solar generation rose 23% and wind by 14% in 2021. Aggregately, this takes them to more than 10% of global electricity generation. All clean electricity sources generated 38% of the world's electricity, more than coal (36%) [3].

In order to increase the total amount of power generation, only increasing the power generation device or improving the energy conversion of the device is insufficient. Perovskite solar cells (PSCs) are photovoltaic (PV) devices capable of converting abundant sunlight radiation into electricity, and they are expected to accelerate the development of renewable energy because of their high conversion efficiency, low production cost, and ease of fabrication [4,5]. In 2009, Kojima et al. pointed out the use of organic–inorganic halide perovskites such as CH<sub>3</sub>NH<sub>3</sub>PbBr<sub>3</sub> (MAPbBr<sub>3</sub>) and CH<sub>3</sub>NH<sub>3</sub>PbI<sub>3</sub> (MAPbI<sub>3</sub>) to enhance the photovoltaic effect in photo electrochemical cells (PECs), with power conversion efficiencies (PCE) of 3.1% and 3.8%, respectively [6], hence, attracting the interest of many researchers around the world, allowing the PCE of PSC to rapidly increase to 25.5% [7].

Optimizing electron and hole-transport materials (ETM and HTM) is a key factor in improving the performance of solar cell devices [8]. In the past, many studies put much effort into optimizing the interface using different materials [9–12]. Recently, perovskite

quantum dots (QDs) have become an alternative HTM, such as the insertion of FAPbX<sub>3</sub> perovskite quantum dot layers to enhance the PCE of PSCs [13]. Subsequently, the perovskite CsPbI<sub>3</sub> QDs, which has the same structure as the emissive layer, has also been investigated as HTL due to its matching energy, high moisture stability [14], and the better stability of all-inorganic materials than organic ones in perovskites [15]. In addition, synthesis methods and ligand exchange engineering for inorganic perovskite CsPbX<sub>3</sub> QDs have been widely studied to improve the photoelectric properties of QDs [16]. However, the ligand exchange of perovskite QD-based HTM for improving interfacial carrier transporting of perovskite solar cells has not yet been discussed.

Accordingly, this study proposes a strategy to optimize interfacial engineering using ligand engineering by replacing the long-chain ligand Oleylamine (OAM) with the short-chain ligand Octylamine (Octam) and introducing the improved QDs into PSCs, thereby improving efficient carrier transport [17,18]. The result showed that QDs with interfacial engineering had higher PCEs compared to PSCs without the interfacial engineering of QDs. This study illustrates an approach to achieve a higher efficiency of PSC.

## 2. Experimental Section

### 2.1. Materials

Cesium carbonate (Cs<sub>2</sub>CO<sub>3</sub>), methyl acetate (MeoAc), and octane (OCT) were acquired from Alfa Aesar. Octadecene (ODE), and oleic acid (OA), Octam, PbI<sub>2</sub>, tetraoctylammonium bromide (TOAB), hexane, and OAM were purchased from Sigma-Aldrich. All other materials and solvents were received from Echo Chemical Co. Ltd. (Miaoli, Taiwan). Besides, CH<sub>3</sub>NH<sub>3</sub>I and ZnO were synthesized using the same method previously published in the literature [19,20].

### 2.2. Synthesis of CsPbI<sub>3</sub> QD Solution

Measures of 320 mg of Cs<sub>2</sub>CO<sub>3</sub>, 9 mL of ODE, and 0.75 mL of OA were loaded into a 50 mL glass bottle and then the solution was heated to dissolve completely using a hotplate stirrer and was vacuumed during the process. Measures of 0.17 g of PbI<sub>2</sub> and 10 mL of ODE were loaded into a glass bottle, and then the solution was heated to dissolve completely with a hotplate stirrer and vacuumed during the process. Then, 1 mL of OA and 1 mL of OAM (or Octam) were injected into the solution and heated to 150 °C for 5 min to prepare CsPbI<sub>3</sub> QDs with OAM ligands (or the short-chain Octam ligands). Afterwards, 0.8 mL of cesium oleate precursor was added into the solution by the rapid hot-injection method and cooled in an ice-water bath to synthesize CsPbI<sub>3</sub> quantum dots. As-prepared solution was added to MeoAc with a volume ratio of 1:1 and centrifuged at 12,000 × g rpm for 10 min. The powder precipitated at the bottom was added to 1 mL of hexane and 3 mL of MeoAc and centrifuged at 12,000 × g rpm for 10 min. Once again, the powder precipitated at the bottom was added to 1 mL of OCT and centrifuged at 12,000 × g rpm for 10 min. Finally, the supernatant was stored at 4 °C until further use.

### 2.3. Device Fabrication

The sol-gel ZnO precursor solution was spin-coated at 5500 rpm for 30 s and annealed at 140 °C for 30 min. Then, the MAPbI<sub>3</sub> perovskite layer was deposited by spin-coating PbI<sub>2</sub> dissolved in dimethylformamide (DMF) (1 mole/L) onto the ZnO layer at 3000 rpm. As the solution dried, CH<sub>3</sub>NH<sub>3</sub>I solution was spin-coated onto PbI<sub>2</sub> at 3000 rpm. More detailed information about the two-step spin coating method has been reported in [21]. Then, CsPbI<sub>3</sub> was spin-coated onto the MAPbI<sub>3</sub> perovskite layer at 2000 rpm for 20 s prior to annealing at 100 °C for 20 s. Afterwards, the sample was successively deposited with molybdenum trioxide (MoO<sub>3</sub>) and Ag cathode by thermal evaporation technique in a high vacuum chamber. The film thickness and deposition rate for the above materials were 5 nm at 0.3 nm/s and 100 nm at 1.5 nm/s, respectively. Eventually, the PSCs were fabricated and encapsulated with a UV-light curing adhesive in a nitrogen-filled glovebox.

## 2.4. Measuring Instruments

The photoluminescence (PL) spectra were measured by a fluorescence spectrophotometer (F-7000, Hitachi, Minato City, Tokyo, Japan). The time-resolved photoluminescence (TRPL) decays were obtained using a HORIBA FluoroMax Plus spectrofluorometer. J-V characteristics.

Solar simulator and EQE spectra were recorded using SS-X Solar system (Enlitech, Kaohsiung, Taiwan) and QE-R quantum efficiency system (Enlitech), respectively. The XRD patterns were analyzed using an X-ray diffractometer (D8 advance, Bruker, Ettlingen, Germany). TEM images with a resolution of  $\leq 0.23$  nm were obtained using a JJ JEM-2100 Plus microscope at an accelerating voltage of 100 kV. The atomic force microscope (AFM) was measured by the tapping mode (INNOVA AFM, Bruker) and has nanometer resolution in the  $x$ - $y$  plane and angstrom resolution in the  $z$ -axis.

## 3. Results and Discussion

In this study, the above synthetic method was used to prepare samples of two CsPbI<sub>3</sub> QD solutions. One is CsPbI<sub>3</sub> QDs with OAM ligands, and the other is CsPbI<sub>3</sub> QDs with Octam ligands through ligand engineering. Both CsPbI<sub>3</sub> QD solutions were purified three times to obtain high quality QDs with a photoluminescence quantum yield (PLQY) of 40.2% and 38.9% for OAM-ligand and Octam-ligand QDs, respectively. To observe the characteristics of the QDs more closely, transmission electron microscopy (TEM) was used to measure the morphology of both QD solutions. Figure 1a shows the crystalline form of QDs with a cubic shape and no aggregation phenomenon was found. Figure 1b presents the size distribution of QDs with OAM and Octam ligands, with standard deviations of 2.3 nm and 3.0 nm, respectively, implying that the QD size distribution is uniform. The average diameters of CsPbI<sub>3</sub> QDs with OAM and Octam ligands were 10.19 nm and 14.37 nm, respectively, and the difference in size was attributed to ligand engineering by replacing the long-chain ligands (OAM) with the short-chain ligands (Octam), resulting in the larger size [22].

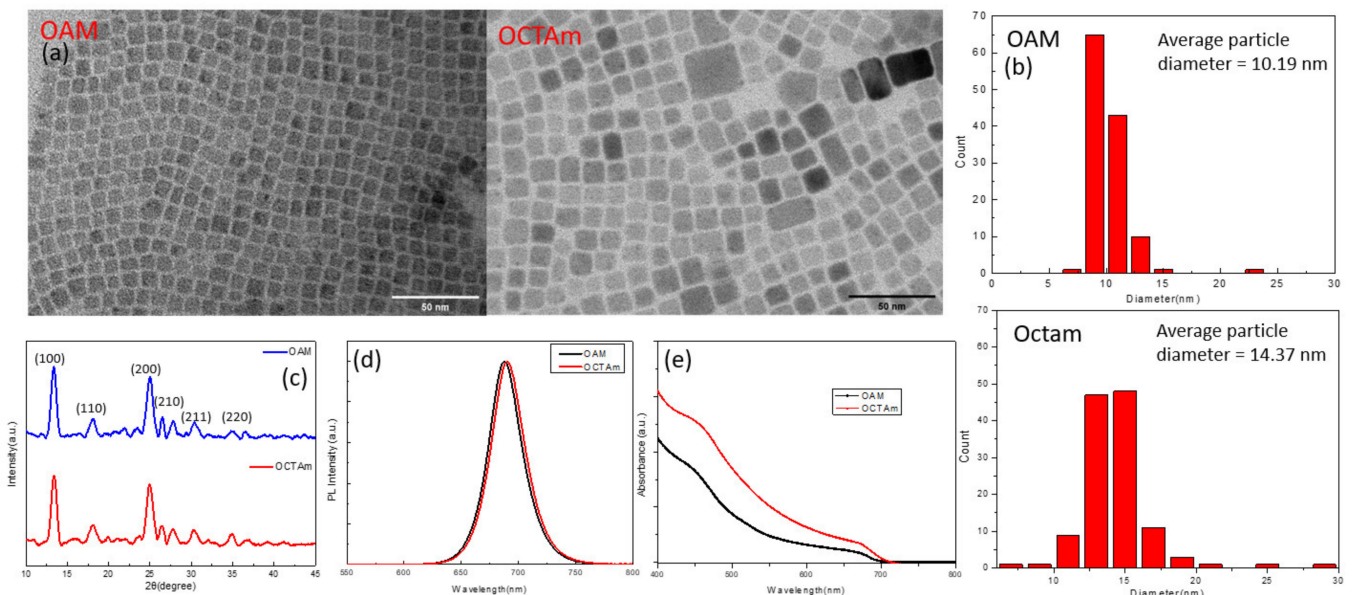


**Figure 1.** (a) TEM images and (b) size distribution for QD films; (c) XRD pattern of CsPbI<sub>3</sub> QDs; (d) PL spectrum and; (e) UV-vis absorbance spectra for QD films.

In addition, the QD structure was further confirmed as a cubic morphology by X-ray diffraction (XRD), and the peak position of the XRD pattern in Figure 1c is consistent with previous study [23]. Figure 1d illustrated the photoluminescence (PL) emission spectrum of the QD solutions and showed the emission peaks at 685 nm (OCTAM ligands) and 690 nm

(OAM ligands), indicating that the CsPbI<sub>3</sub> QDs were obtained using both ligands. The CsPbI<sub>3</sub> QDs with OCTAm ligands are slightly red-shifted compared to the CsPbI<sub>3</sub> QDs with OAM ligands in the PL spectrum, which is caused by the size-up of the QDs and corresponds to the TEM images [24]. However, the ultraviolet–visible (UV–vis) absorbance spectra in Figure 1e exhibit that both QD solutions are absorbed in the visible spectrum, which can enhance the light absorption of PSC [13]. The band gaps for the OAM- and OCTAm-based CsPbI<sub>3</sub> QDs can be calculated as 1.84 eV and 1.85 eV through the UV-vis absorbance spectra (see Supplementary Materials Figure S1), respectively, which is also in agreement with the previous study [25,26].

According to the results of the above analyses, the high-quality QD solutions were synthesized and then introduced the QDs between HTM and perovskite film for PSCs by interfacial engineering. In the study, the schematic structure of the PSC is shown in Figure 2a, which consists of a multilayer structure ITO/ZnO/MAPbI<sub>3</sub>/QD/MoO<sub>3</sub>/Ag. For further investigation of the QDs on MAPbI<sub>3</sub> perovskite film, a scanning electron microscope (SEM) was used to measure MAPbI<sub>3</sub> before and after being coated with the QDs and found that MAPbI<sub>3</sub> perovskite film without QDs showed a clear crystal structure, as shown in Figure 2b. However, the QDs using OAM ligands appear granular on the MAPbI<sub>3</sub> perovskite film in Figure 2b. In contrast, the QDs using Octam ligands showed a smooth and uniform surface of MAPbI<sub>3</sub> film. A similar observation was obtained in the atomic force microscope (AFM) measurement in Figure 2c, which is identical to the SEM images in Figure 2b. The QDs using Octam ligands showed a uniform distribution on MAPbI<sub>3</sub> perovskite film compared to the QDs using OAM ligands, and their root-mean-square roughness ( $S_q$ ) was 57 nm and 83 nm, respectively.

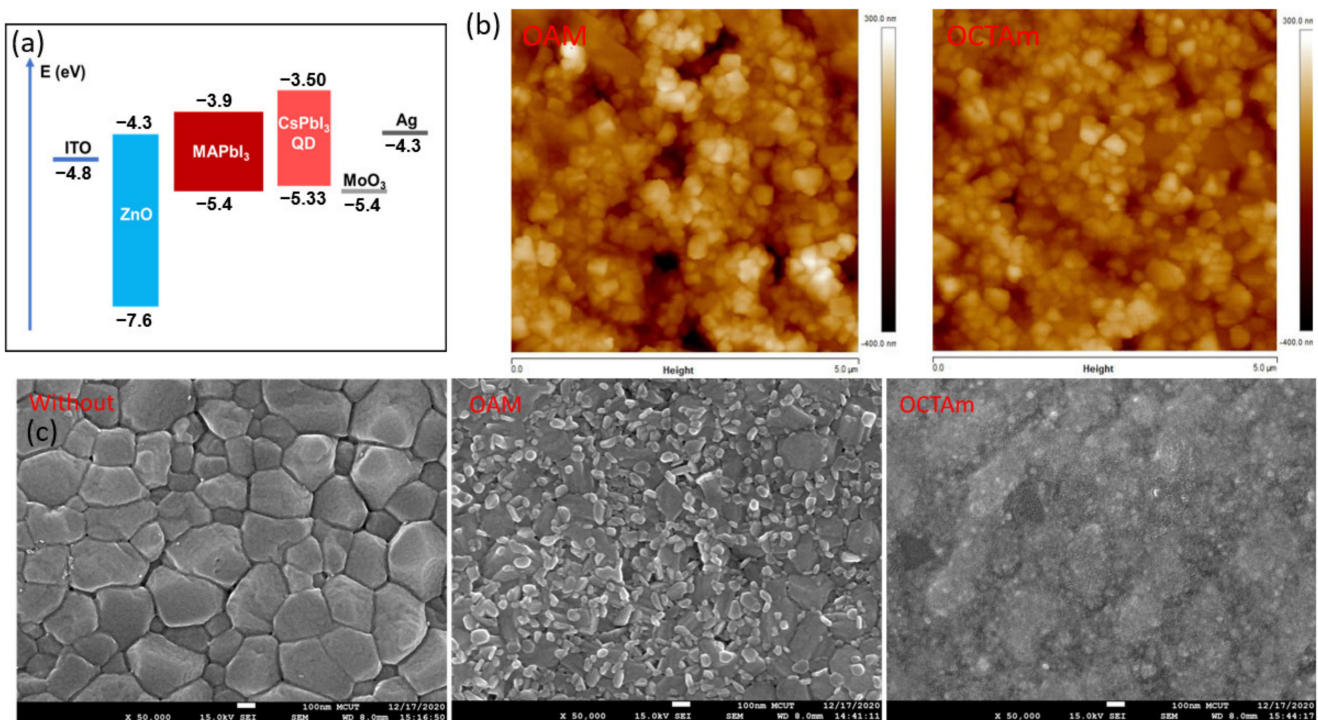


**Figure 2.** (a) The energy level diagram of PSC; (b) SEM and (c) AFM images of MAPbI<sub>3</sub> films.

It is well known the matching energy levels can optimize the performance of the PSCs [27]. Therefore, in this study, the energy-level matched QDs between MoO<sub>3</sub> (hole injection layer) [28] and perovskite MAPbI<sub>3</sub> films were introduced through interfacial engineering to increase the hole transfer without significant energy loss in order to improve the efficiency in the hole-transport layer, as shown in Figure 2a [29]. To verify the effect of QDs on PSC and the importance of matching energy levels, this study experimentally

fabricated three types of PSCs, one without QD coating, another with QDs using OAM ligands, and the other with QDs using Octam ligands. Interestingly, the PSC coated with the QDs using OAM ligands failed in measurement, implying that this PSC cannot conduct current. This phenomenon can be attributed to two possibilities. One is that the QDs using long-chain insulating ligands hinder carrier transport in device applications [30]. The other possibility is that the QD coating cannot form a film on the MAPbI<sub>3</sub> layer, leading to an increase in surface defects, resulting in defects of trap free charges and reducing the current density, leading to a lower luminance [31]. This result also matches with Figure 2b. Consequently, the traditional long-chain OAM ligand on the QDs cannot form a full coverage film on the MAPbI<sub>3</sub> layers, but the short-chain Octam ligands can be used as the suitable HTM. In this way, the disadvantage of conductivity can be solved and the formation of the surface film can be more uniform and smoother in Figure 2c, thus improving the efficiency of hole transport through ligand engineering.

Figure 3a presents the current-voltage (J-V) characteristics for the PSC without QD coating and the one coated with QDs using Octam ligands. It is shown that the PSC coated with QDs using Octam ligands exhibited significant improvement in photovoltaic performance. The open-circuit voltage increased from 1.03 to 1.09 volts, the short-circuit current increased from 19.8 to 20.5 mA/cm<sup>2</sup>, and the fill factor (FF) increased from 68.7% to 75.7%, corresponding to an increase in power conversion efficiency (PCE) from 14.1% to 17.0%. It can be seen that introducing QDs enhances the carrier mobility through the interfacial engineering to make the energy levels matching, so that PSC with QDs using Octam ligands can obtain higher open-circuit voltage, short-circuit current, and further improve the PCE. Figure 3b showed the EQE spectrum of the PSC with QDs using Octam ligands, where the maximum EQE of that reached 79.7%.

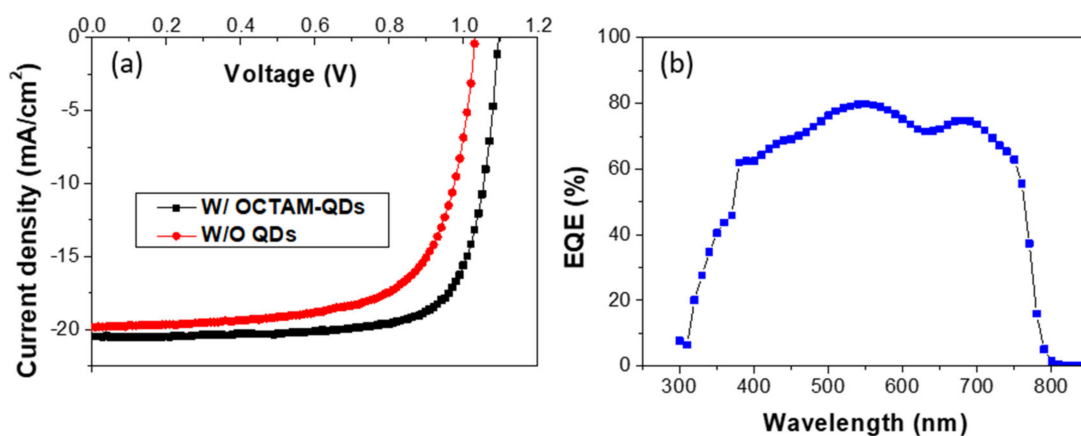


**Figure 3.** (a) J-V characteristics for PSCs and (b) EQE spectrum of the PSC with QDs using Octam ligands.

For further examination of the photovoltaic performance of PSC improved by introducing QDs, the absorbance of MAPbI<sub>3</sub> films with and without QDs was measured, and it was found that the absorbance of the film with QDs was significantly enhanced over that of the film without QDs in the range from 500 nm to 750 nm. Similarly, QDs also showed a slight signal in the absorbance between 500 nm to 700 nm in Figure 4a. Furthermore, the PL spectra of the MAPbI<sub>3</sub> films with and without QDs were measured in Figure 4b to demonstrate that introducing QDs improved the charge transfer, and there was no obvious shift in the peak position, but a difference in PL intensity. The PL intensity of MAPbI<sub>3</sub> film with QDs was 30% lower than that without QDs, which could be attributed to the charge carrier extraction enhanced by the introduction of QDs [14]. We carried out the time-resolved photoluminescence (TRPL) measurement to investigate the effect of QDs on the hole extraction kinetics at the interface between MAPbI<sub>3</sub> and HTM layers. Figure 4c showed the decay lifetime of the MAPbI<sub>3</sub> film without QDs is 110 ns, but that of the MAPbI<sub>3</sub> film with QDs is greatly shortened to 88 ns, indicating a rapid charge transfer

from perovskite material to HTM [32]. As a result, the PSCs with QDs possess better performance in PCE than those without QDs.

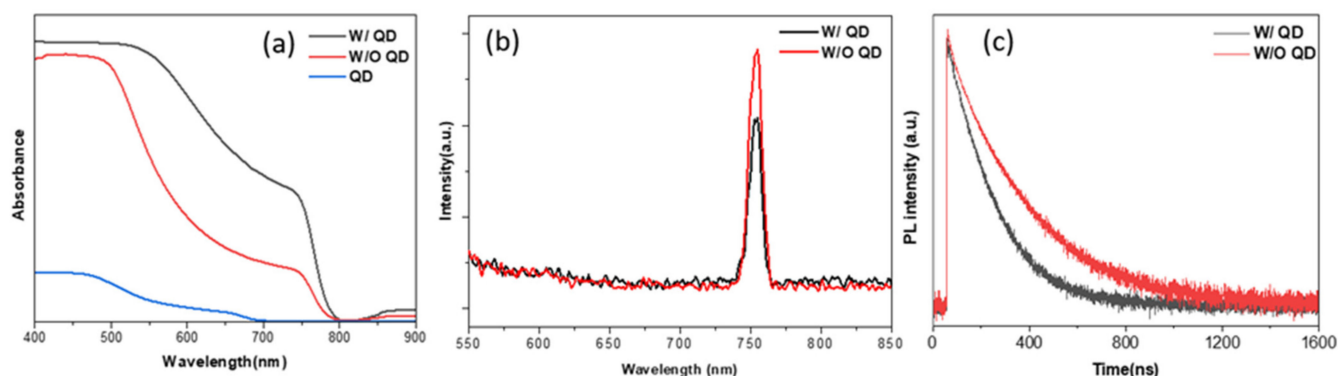


**Figure 4.** (a) The absorbance spectra; (b) PL spectrum; and (c) TRPL decay curves for MAPbI<sub>3</sub> films.

#### 4. Conclusions

This study has examined the effects of perovskite CsPbI<sub>3</sub> QDs via the ligand engineering as an HTL of a planar PSC. The optimal open-circuit voltage has been shown as 1.09 V, the short-circuit current as 20.5 mA/cm<sup>2</sup>, and the fill factor (FF) as 75.7%, and the power conversion efficiency (PCE) as 17.0% of the device. As a result, introducing QDs as a HTL via the ligand engineering can effectively improve the device performance of the PSC. In general, this study has shown that ligand engineering is a candidate for optimizing interfacial characteristic of the PSC.

**Supplementary Materials:** The following supporting information can be downloaded at: <https://www.mdpi.com/article/10.3390/ma15248902/s1>, Figure S1: The tau's plot of the QDs with OAM and Octam ligands.

**Author Contributions:** Conceptualization, L.-C.C. and C.-C.L.; formal analysis, T.-T.K.; investigation, S.-A.C., C.-Y.C. and C.-H.C.; methodology, S.-A.C. and Y.-J.C.; resources, L.-C.C.; writing—original draft, T.-C.L. and H.-Y.S.; writing—review & editing, C.-C.L. All authors have read and agreed to the published version of the manuscript.

**Funding:** This work was supported by the National Science and Technology Council, Taiwan, under Grant No. NSTC 111-2221-E-131-031.

**Institutional Review Board Statement:** Not applicable.

**Informed Consent Statement:** Not applicable.

**Data Availability Statement:** Data sharing not applicable.

**Acknowledgments:** The authors would like to thank the members of the Organic Electronics Research Center, Ming Chi University of Technology, for valuable and significant assistance.

**Conflicts of Interest:** The authors declare no conflict of interest.

#### References

1. Paramati, S.R.; Shahzad, U.; Dogan, B. The role of environmental technology for energy demand and energy efficiency: Evidence from OECD countries. *Renew. Sustain. Energy Rev.* **2022**, *153*, 111735. [CrossRef]
2. Bouckaert, S.; Pales, A.F.; McGlade, C.; Remme, U.; Wanner, B.; Varro, L.; D'Ambrosio, D.; Spencer, T. *Net Zero by 2050, a Roadmap for the Global Energy Sector*; IEA: Paris, France, 2021.
3. Jones, D. *Global Electricity Review 2022*; Ember: London, UK, 2022.
4. Lee, M.M.; Teuscher, J.; Miyasaka, T.; Murakami, T.N.; Snaith, H.J. Efficient Hybrid solar cells based on meso-superstructured organometal halide perovskites. *Science* **2012**, *338*, 643–647. [CrossRef]
5. Kim, J.Y.; Lee, J.W.; Jung, H.S.; Shin, H.; Park, N.G. High-efficiency perovskite solar cells. *Chem. Rev.* **2020**, *120*, 7867–7918. [CrossRef] [PubMed]

6. Kojima, A.; Teshima, K.; Shirai, Y.; Miyasaka, T. Organometal halide perovskites as visible-light sensitizers for photovoltaic cells. *J. Am. Chem. Soc.* **2009**, *131*, 6050–6051. [[CrossRef](#)] [[PubMed](#)]
7. Green, M.; Dunlop, E.; Hohl-Ebinger, J.; Yoshita, M.; Kopidakis, N.; Hao, X. Solar cell efficiency tables (version 57). *Prog. Photovolt. Res. Appl.* **2021**, *29*, 3–15. [[CrossRef](#)]
8. Adhyaksa, G.W.P.; Veldhuizen, L.W.; Kuang, Y.; Brittan, S.; Schropp, R.E.I.; Garnett, E.C. Carrier diffusion lengths in hybrid perovskites: Processing, composition, aging, and surface passivation effects. *Chem. Mater.* **2016**, *28*, 5259–5263. [[CrossRef](#)]
9. Kim, H.S.; Lee, C.R.; Im, J.H.; Lee, K.B.; Moehl, T.; Marchioro, A.; Moon, S.J.; Humphry-Baker, R.; Yum, J.H.; Moser, J.E.; et al. Lead iodide perovskite sensitized all-solid-state submicron thin film mesoscopic solar cell with efficiency exceeding 9%. *Sci. Rep.* **2012**, *2*, 591. [[CrossRef](#)] [[PubMed](#)]
10. Malinkiewicz, O.; Yella, A.; Lee, Y.H.; Espallargas, G.M.; Graetzel, M.; Nazeeruddin, M.K.; Bolink, H.J. Perovskite solar cells employing organic charge-transport layers. *Nat. Photonics* **2014**, *8*, 128–132. [[CrossRef](#)]
11. Christians, J.A.; Fung, R.C.M.; Kamat, P.V. An inorganic hole conductor for organo-lead halide perovskite solar cells. Improved hole conductivity with copper iodide. *J. Am. Chem. Soc.* **2014**, *136*, 758–764. [[CrossRef](#)]
12. Heo, J.H.; Im, S.H.; Noh, J.H.; Mandal, T.N.; Lim, C.S.; Chang, J.A.; Lee, Y.H.; Kim, H.; Sarkar, A.; Nazeeruddin, M.K.; et al. Efficient inorganic–organic hybrid heterojunction solar cells containing perovskite compound and polymeric hole conductors. *Nat. Photonics* **2013**, *7*, 486–491. [[CrossRef](#)]
13. Chen, L.-C.; Tien, C.-H.; Tseng, Z.-L.; Ruan, J.-H. Enhanced Efficiency of MAPbI<sub>3</sub> Perovskite Solar Cells with FAPbX<sub>3</sub> Perovskite Quantum Dots. *Nanomaterials* **2019**, *9*, 121. [[CrossRef](#)] [[PubMed](#)]
14. Liu, C.; Hu, M.; Zhou, X.; Wu, J.; Zhang, L.; Kong WLi, X.; Zhao, X.; Dai, S.; Xu, B.; Cheng, C. Efficiency and stability enhancement of perovskite solar cells by introducing CsPbI<sub>3</sub> quantum dots as an interface engineering layer. *NPG Asia Mater.* **2018**, *10*, 552–561. [[CrossRef](#)]
15. Luo, P.; Xia, W.; Zhou, S.; Sun, L.; Cheng, J.; Xu, C.; Lu, W. Solvent engineering for ambient-air-processed, phase-stable CsPbI<sub>3</sub> in perovskite solar cells. *J. Phys. Chem. Lett.* **2016**, *7*, 3603–3608. [[CrossRef](#)] [[PubMed](#)]
16. Chiba, T.; Kido, J. Lead halide perovskite quantum dots for light-emitting devices. *J. Mater. Chem. C* **2018**, *6*, 11868–11877. [[CrossRef](#)]
17. Dai, J.; Xi, J.; Li, L.; Zhao, J.; Shi, Y.; Zhang, W.; Ran, C.; Jiao, B.; Hou, X.; Duan, X.; et al. Charge transport between coupling colloidal perovskite quantum dots assisted by functional conjugated ligands. *Angew. Chem. Int. Ed.* **2018**, *57*, 5754–5758. [[CrossRef](#)] [[PubMed](#)]
18. Liu, Y.; Gibbs, M.; Puthussery, J.; Gaik, S.; Ihly, R.; Hillhouse, H.W.; Law, M. Dependence of carrier mobility on nanocrystal size and ligand length in PbSe nanocrystal solids. *Nano Lett.* **2010**, *10*, 1960–1969. [[CrossRef](#)] [[PubMed](#)]
19. Tseng, Z.L.; Chiang, C.H.; Wu, C.G. Surface engineering of ZnO thin film for high efficiency planar perovskite solar cells. *Sci. Rep.* **2015**, *5*, 13211. [[CrossRef](#)]
20. Chen, L.C.; Tseng, Z.L.; Lin, C.C. Low-temperature sol–gel derived ZnO films as electron transporting layers for perovskite-based solar cells. *J. Nanoelectron. Optoelectron.* **2019**, *14*, 723–728. [[CrossRef](#)]
21. Chiang, C.H.; Tseng, Z.L.; Wu, C.G. Planar heterojunction perovskite/PC<sub>71</sub>BM solar cells with enhanced open-circuit voltage via a (2/1)-step spin-coating process. *J. Mater. Chem. A* **2014**, *2*, 15897–15903. [[CrossRef](#)]
22. Kim, Y.H.; Lee, G.H.; Kim, Y.T.; Wolf, C.; Yun, H.J.; Kwon, W.; Park, C.G.; Lee, T.W. High efficiency perovskite light-emitting diodes of ligand-engineered colloidal formamidinium lead bromide nanoparticles. *Nano Energy* **2017**, *38*, 51–58. [[CrossRef](#)]
23. Lu, C.; Wright, M.; Ma, X.; Li, H.; Itanze, D.; Carter, J.A.; Hewitt, C.A.; Donati, G.L.; Carroll, D.L.; Lundin, P.M.; et al. Cs oleate precursor preparation for lead halide perovskite nanocrystal synthesis: The influence of excess oleic acid on achieving solubility, conversion, and reproducibility. *Chem. Mater.* **2018**, *31*, 62–67. [[CrossRef](#)]
24. Xu, F.; Kong, X.; Wang, W.; Juan, F.; Wang, M.; Wei, H.; Li, J.; Cao, B. Quantum size effect and surface defect passivation in size-controlled CsPbBr<sub>3</sub> quantum dots. *J. Alloys Compd.* **2020**, *831*, 154834. [[CrossRef](#)]
25. Tauc, J.; Grigorovici, R.; Vancu, A. Optical properties and electronic structure of amorphous germanium. *Phys. Status Solidi B* **1966**, *15*, 627–637. [[CrossRef](#)]
26. Wu, Y.; Yang, X.; Chen, W.; Yue, Y.; Cai, M.; Xie, F.; Bi, E.; Islam, A.; Han, L. Perovskite solar cells with 18.21% efficiency and area over 1 cm<sup>2</sup> fabricated by heterojunction engineering. *Nat. Energy* **2016**, *1*, 16148. [[CrossRef](#)]
27. Malinkiewicz, O.; Roldán-Carmona, C.; Soriano, A.; Bandiello, E.; Camacho, L.; Nazeeruddin, M.K.; Bolink, H.J. Metal-oxide-free methylammonium lead iodide perovskite-based solar cells: The influence of organic charge transport layers. *Adv. Energy Mater.* **2014**, *4*, 1400345. [[CrossRef](#)]
28. Giroto, C.; Voroshazi, E.; Cheyns, D.; Heremans, P.; Rand, B.P. Solution-Processed MoO<sub>3</sub> Thin Films As a Hole-Injection Layer for Organic Solar Cells. *ACS Appl. Mater. Interfaces* **2011**, *3*, 3244–3247. [[CrossRef](#)]
29. Schulz, P.; Edri, E.; Kirmayer, S.; Hodes, G.; Cahen, D.; Kahn, A. Interface energetics in organo-metal halide perovskite-based photovoltaic cells. *Energy Environ. Sci.* **2014**, *7*, 1377–1381. [[CrossRef](#)]
30. Tseng, Z.L.; Huang, Y.S.; Liu, Y.L.; Wu, T.L.; Wei, Y.J. Tetraoctylammonium bromide-passivated CsPbI<sub>3-x</sub>Br<sub>x</sub> perovskite nanoparticles with improved stability for efficient red light-emitting diodes. *J. Alloys Compd.* **2022**, *897*, 163182. [[CrossRef](#)]

31. Yang, Z.; Wang, W.; Pan, J.; Ye, C. Alternating current electroluminescent devices with inorganic phosphors for deformable displays. *Cell Rep. Phys. Sci.* **2020**, *1*, 100213. [[CrossRef](#)]
32. Rakstys, K.; Abate, A.; Dar, M.I.; Gao, P.; Jankauskas, V.; Jacopin, G.; Kamarauskas, E.; Kazim, S.; Ahmad, S.; Grätzel, M.; et al. Triazatruxene-based hole transporting materials for highly efficient perovskite solar cells. *J. Am. Chem. Soc.* **2015**, *137*, 16172–16178. [[CrossRef](#)] [[PubMed](#)]